IL NUOVO CIMENTO Vol. 37 C, N. 2 Marzo-Aprile 2014
DOI 10.1393/ncc/i2014-11755-9

Colloquia: LC13

Measurement of pp inelastic cross section at $\sqrt{s} = 7\,\text{TeV}$ at LHC

S. Valentinetti
INFN, Sezione di Bologna and Università di Bologna - Bologna, Italy

ricevuto il 4 Febbraio 2014

Summary. — pp interactions can be cathegorized, according to their final state, as elastic, diffractive inelastic and inelastic. If the mass of the final state is small ($M_x < 15\,\text{GeV}$) the event escapes undetected. Both CMS and ATLAS measured the total inelastic cross section for M_x greater than 15.7 GeV with good precision and then extrapolated it to the full mass range using Monte Carlo models. The results of the total inelastic pp cross section at $\sqrt{s} = 7\,\text{TeV}$ and the extrapolated value are here presented for both experiments. The ATLAS measurement of the inelastic cross section as a function of the rapidity gap, used to tune the MC simulations in the low mass region, is also presented.

PACS 13.75.Cs – Nucleon-nucleon interactions (including antinucleons, deuterons, etc.).
PACS 25.40.Ep – Inelastic proton scattering.

1. – Introduction

At LHC energies the largest contribution to the total pp cross section, composed by the elastic and inelastic part, is due to inelastic processes, that can be separated in non-diffractive (ND), single diffractive (SD), double diffractive (DD) and central diffractive (CD) components. The diffractive processes are characterized by a final state in which the produced particles are separated in rapidity η([1]) by a gap due to the exchange of a gluon ladder. The size of the gap is related to the mass of the dissociative system M_x (*i.e.* in case of single diffraction $\Delta\eta \propto \ln\xi$, where $\xi = M_x^2/s$ with s the centre of mass energy). Since both CMS [1] and ATLAS [2] were designed to be highly sensitive to high-p_T physics (high final state mass) and did not cover the whole rapidity range, only the measurement of the inelastic cross section in the mass range given by the detector acceptance $M_x > 15.7\,\text{GeV}$ was performed. The measurement was then extrapolated to

([1]) $\eta = -\ln[\tan(\theta \setminus 2)]$, where θ is the polar angle in a right-handed coordinate system with the origin at the interaction point, the z-axis coincides with the beam line and the x-axis points to the centre of the LHC ring.

the full mass range by using Monte Carlo (MC) simulations. The measured inelastic pp cross section served as an input to validate the phenomenological models and provided basic information needed for tuning Monte Carlo (MC) generators.

2. – Measurement of pp inelastic cross section at $\sqrt{s} = 7\,\text{TeV}$ with CMS

CMS measured the total inelastic cross section using two different methods [3]. In the first method, called *Event Counting*, events triggered by at least one of the Hadron Forward Calorimeters (HF) ($2.9 < |\eta| < 5.2$) were counted. In the second method, called *Pile-up Counting*, the number of pile-up events triggered by the inner tracker ($|\eta| < 2.4$) in a given bunch crossing was counted as a function of bunch luminosity. For these analyses seven runs taken in 2010 at $\sqrt{s} = 7\,\text{TeV}$ at different values of average number of collisions per bunch crossing (from 0.007 to 0.1) were used.

Event counting method. In this method [4] the number of events that deposited at least 5 GeV of energy in any of the two HF calorimeters were counted. The HF acceptance $2.9 < |\eta| < 5.2$ corresponded to the kinematic range $\xi < 5 \cdot 10^{-6}$. In this range the inelastic cross section was evaluated as

$$\sigma_{inel}^{pp}(\xi < 5 \cdot 10^{-6}) = \frac{N_{inel}(1 - f_{\xi<5\cdot10^{-6}})F_{pile-up}}{\epsilon_\xi \cdot L_{int}}\,, \tag{1}$$

N_{inel} was the number of selected events, background subtracted. $F_{pile\text{-}up}$ was the pile-up correction factor: since the acceptance of the calorimeters was outside the acceptance of the tracker, events with more than one interaction in the same bunch crossing cuold not be discarted and a pile-up correction was necessary. $F_{pile\text{-}up}$ was evaluated from data using the ratio of the number of detected events to the number of triggers counted requiring the coincidence of the two HF calorimeters. The detection efficiency ϵ_ξ and the contamination factors $f_{\xi<5\cdot10^{-6}}$ (fraction of selected events with low mass ≈ 0.02) were determined using three MC generators (PHYTIA6, PYTHIA8 and PHOJET) with an estimated uncertainties at 1% level [4]. The expected distributions of the kinematic variable ξ for all events, events that deposit 4 GeV and 5 GeV of energy in the HF, respectively, are shown as a function of the kinematic variable ξ in fig. 1. The cut on $\xi > 5 \cdot 10^{-6}$ for $E_{HF} > 5\,\text{GeV}$ guaranteed that more than 98% of total events were detected. The final inelastic cross section value, obtained averaging the cross sections measured in runs at different pile-up conditions and shown in fig. 2, was

$$\sigma_{inel}^{pp}(\xi > 5 \cdot 10^{-6}) = 60.2 \pm 0.2(\text{stat}) \pm 1.1(\text{syst}) \pm 2.4(\text{lumi})\,\text{mb}. \tag{2}$$

Pile-up counting method. This analysis [5] was based on the assumption that the number of inelastic pp interactions (n) in a given bunch crossing was a function of the total inelastic cross section σ_{inel} via the Poisson probability distribution function $P(n)$:

$$P(n) = \frac{(L \cdot \sigma_{inel})^n}{n!} \cdot e^{-L\cdot\sigma_{inel}} \tag{3}$$

where L was the bunch luminosity. The number of reconstructed vertices that fulfilled quality requirements were counted at each bunch crossing. To obtain the true number of vertices a bin-by-bin correction was applied to the visible number of vertices using

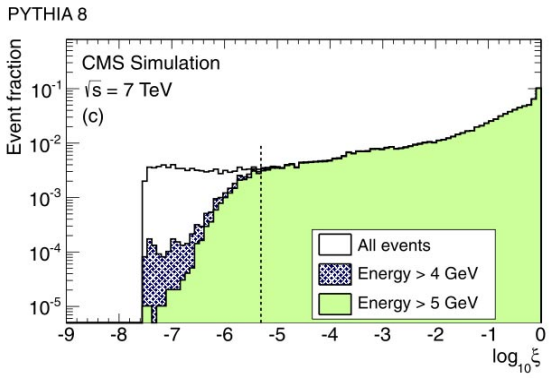

Fig. 1. – Simulated distributions of the kinematic variable ξ for all events (white), events that deposit $E_{HF} > 4\,\text{GeV}$ (blue), studied for systematic effects, and $E_{HF} > 5\,\text{GeV}$ (green) for the full mass range. The cut on $\xi > 5 \cdot 10^{-6}$ (dashed vertical line) guarantees that more than 98% of total events are detected.

MC simulation. This accounted for vertex reconstruction efficiency, vertex merging and fakes. After the correction, the distributions of the fraction of pile-up events as a function of luminosity for $n = 0 \ldots 8$ pile-up events were fitted with a Poisson distribution. The final value of the inelastic cross section was evaluated by averaging the nine values of visible cross section, as shown in fig. 3. The analysis was performed by using three sets of events, requiring respectively at least 1, 2 or 3 tracks for each vertex. The results for the different samples were

$$\sigma_{vis}^{pp}(\geq 1 \text{ track}) = 58.7 \pm 2.0(\text{syst}) \pm 2.4(\text{lumi})\,\text{mb},$$
$$\sigma_{vis}^{pp}(\geq 2 \text{ track}) = 57.2 \pm 2.0(\text{syst}) \pm 2.4(\text{lumi})\,\text{mb},$$
$$\sigma_{vis}^{pp}(\geq 3 \text{ track}) = 55.4 \pm 2.0(\text{syst}) \pm 2.4(\text{lumi})\,\text{mb}. \tag{4}$$

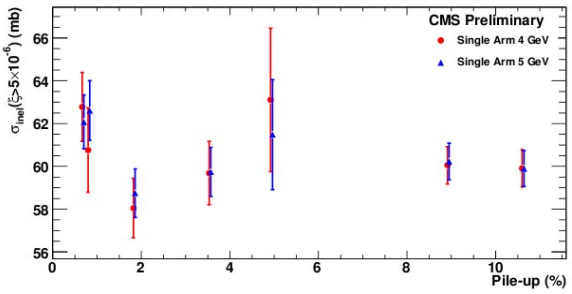

Fig. 2. – Inelastic pp cross section at 7 TeV for $\xi > 5 \cdot 10^{-6}$ obtained from data sets collected at various pile-up conditions. The error bars show the statistical uncertainties combined with the systematic ones. The final result of the cross section is obtained averaging the seven values at 5 GeV.

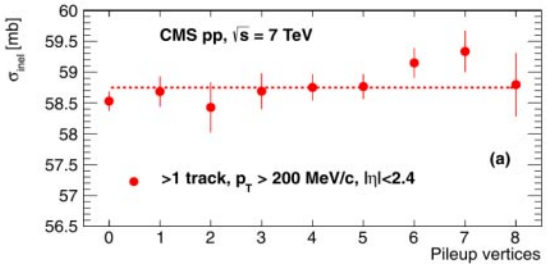

Fig. 3. – Visible inelastic pp cross section as a function of the number of pile-up vertices, in events with at least one track with $p_T > 200$ MeV and $|\eta| < 2.4$ for each vertex. The line is the result of averaging the nine individual values of cross section.

Extrapolation to the total inelastic cross section. Six different MC generators were used to extrapolate the visible inelastic cross section to the total inelastic cross section, in the full mass range. All models showed similar trend for cross section at the measured hadron level but there were substantial differences in the expectations for the total inelastic pp cross section, as visible in fig. 4. The final extrapolated values of the inelastic cross section for the two analyses were respectively:

$$\sigma_{inel}^{pp}(7\,\text{TeV}) = 64.5 \pm 0.2(\text{stat}) \pm 1.1(\text{syst}) \pm 2.4(\text{lumi}) \pm 1.5(\text{extr})\,\text{mb}, \tag{5}$$

$$\sigma_{inel}^{pp}(7\,\text{TeV}) = 68.0 \pm 2.0(\text{syst}) \pm 2.4(\text{lumi}) \pm 4.0(\text{extr})\,\text{mb}.$$

The largest uncertainty came from extrapolation and was greater for the pile-up method for which the detector acceptance was smaller.

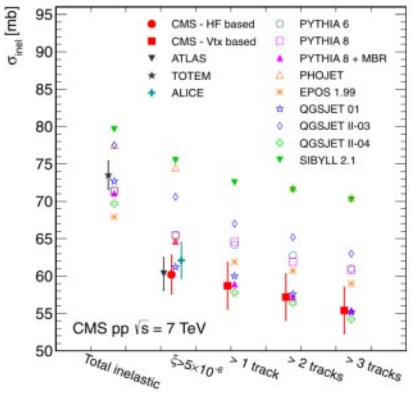

Fig. 4. – Inelastic cross section extrapolated to the full mass range (first column) and measured with the event counting method (red filled circle, second column) and with the pile-up counting method (red squares, last three columns for three data sets). Other LHC experimental results are also presented. Data are compared to different MC generators with uncertainty of 1 mb (not shown).

3. – Measurement of pp inelastic cross section at $\sqrt{s} = 7\,\text{TeV}$ with ATLAS

To measure the inelastic cross section ATLAS used events triggered by the Minimum Bias Trigger Scintillator detector (MBTS), composed by two sets of scintillator counters situated on the inner face of the endcap calorimeters in the forward region of ATLAS. MBTS, the Inner Detector (ID) and the calorimeters covered together the pseudorapidity range of $|\eta| < 4.9$, corresponding to $\xi > 5 \cdot 10^{-6}$ and $M_x > 15.7\,\text{GeV}$. The detector acceptance didn't permit the detection of events at low mass. To extrapolate to the full mass range, data were corrected using MC simulations, that had to be validated by data themselves.

Total inelastic cross section. The data considered in this analysis [6] were collected during a single fill in 2010 at a centre of mass energy of 7 TeV, corresponding to an integrated luminosity of $20.3 \pm 0.7\,\mu\text{b}^{-1}$, and with an average number of collisions per bunch crossing of 0.01, triggered by MBTS. Two samples were used: the inclusive, in which MBTS activity was required on any of the two detector sides, and the single side, in which activity was required on one side only. The inelastic cross section in the detector acceptance was evaluated as

$$\sigma_{inel}^{pp}(\xi > 5 \cdot 10^{-6}) = \frac{N - N_{bkg}}{\epsilon_{trigg} \cdot L_{int}} \times \frac{1 - f_{\xi<5\cdot10^{-6}}}{\epsilon_{sel}}\,, \tag{6}$$

where N and N_{bkg} were the number of selected and background events respectively, ϵ_{trigg} was the trigger efficiency (about 99.98% from MC simulations), L_{int} was the integrated luminosity, $f_{\xi<5\cdot10^{-6}}$ was the contamination as defined for CMS and ϵ_{sel} was the offline event selection efficiency (100% for $\xi > 5 \cdot 10^{-6}$). To reduce the uncertainties due to the dependence on MC generators, the fraction of diffractive events (*i.e.* the relative diffraction dissociation cross section), defined as

$$f_D = \frac{\sigma_{SD} + \sigma_{DD} + \sigma_{CD}}{\sigma_{inel}}\,, \tag{7}$$

was constrained by using the measurement of the ratio of single side to inclusive events $R_{SS} = N_{SS}/N_{incl}$ as shown in fig. 5. The fraction of dissociative events was estimated to be $26.9^{+2.5}_{-1.0}\%$.

The final value of the inelastic cross section inside the ATLAS acceptance was

$$\sigma_{inel}^{pp}(\xi > 5 \cdot 10^{-6}) = 60.3 \pm 0.05(\text{stat}) \pm 0.5(\text{syst}) \pm 2.1(\text{lumi})\,\text{mb} \tag{8}$$

and the one extrapolated to the full kinematic range was

$$\sigma_{inel}^{pp}(7\,\text{TeV}) = 69.1 \pm 2.4(\text{exp}) \pm 6.9(\text{extr})\,\text{mb}. \tag{9}$$

These results are shown in fig. 6, where the present results are compared to the measurements obtained with previous experiments [8] and with different theoretical predictions [9-11].

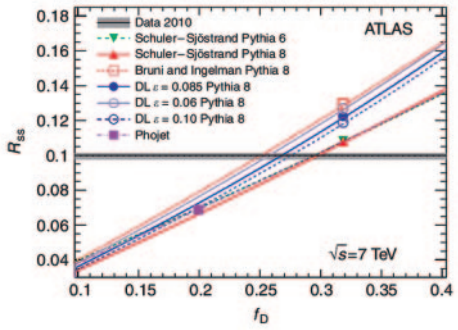

Fig. 5. – Measured value of R_{SS} presented as the grey horizontal line (systematic uncertainties). Predictions of several models are shown as a function of assumed relative diffractive contribution (f_D) indicated by the markers. The value of f_D that best match the value of R_{SS} is $26.9^{+2.5}_{-1.0}\%$ when the Donnachie-Landshoff model (DL, blue filled circle) is used.

Rapidity gap cross section. To extrapolate the inelastic cross section to the low mass range where ATLAS didn't have rapidity acceptance, different MC models were used. ATLAS performed a measurement of the differential inelastic cross section as a function of the rapidity gap [12] used to validate the MC models of diffractive processes. For this analysis data collected in a single run in 2010 at $\sqrt{s} = 7\,\text{TeV}$ with a negligible pile-up contamination and at an integrated luminosity of $7\,\mu\text{b}^{-1}$ were used. The events were studied as a function of the largest forward rapidity gap defined as follow: the calorimeters and ID acceptance was divided into unit-$\Delta\eta$ rings starting from the edge of the detector ($\eta = \pm 4.9$); the observable forward rapidity gap $\Delta\eta^F$ was defined as the largest of the forward rapidity regions, from the edge of the detector to the nearest track or calorimeter cluster, in which no ring presented activity. The differential inelastic cross section as a function of $\Delta\eta^F$ is shown in fig. 7 for particles with $p_T > 200\,\text{MeV}$. The data were compared with PYTHIA8 predictions showing separately the contributions of the different non diffractive and diffractive processes. At small values of $\Delta\eta^F$, the cross sec-

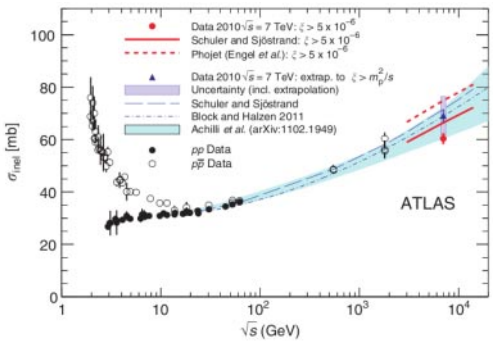

Fig. 6. – Inelastic cross section *versus* the centre of mass energy. The ATLAS measurement for $\xi > 5 \cdot 10^{-6}$ is shown as red filled circle and compared with the predictions of different models. The extrapolation to the full kinematic range is presented as blue filled triangle. Data from different experiments are shown as filled circles for pp and unfilled circles for $p\overline{p}$.

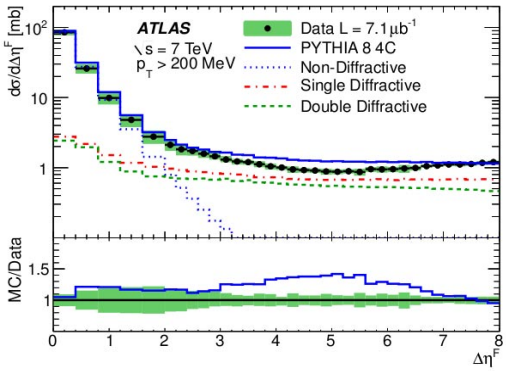

Fig. 7. – Inelastic cross section as function of the forward rapidity gap for particles with $p_T > 200\,\text{MeV}$. The data are compared with PYTHIA8 predictions showing separately the different diffractive components.

tion was dominated by the non diffractive component, that was exponentially suppressed as $\Delta\eta^F$ increases. For intermediate values of $\Delta\eta^F$ (from two to five), the differential cross section showed a *plateau*. At high $\Delta\eta^F$ (> 5) the cross section presented a rise due to the diffractive components only. No MC model predicted the data distribution perfectly: the comparison of different MCs over a large rapidity region allowed ATLAS to tune the relative fractions of the different diffractive components. The differential cross section integrated on ξ over ATLAS mass range is presented in fig. 8: the data were compared to the predictions for $\xi > 5 \cdot 10^{-6}$. ATLAS results were shown together with TOTEM ones, covery the low mass region ($\xi < 10^{-6}$) [13].

4. – Conclusions

CMS and ATLAS measurements of the pp inelastic cross section at $\sqrt{s} = 7\,\text{TeV}$ in the detector acceptance range that corresponded to a final-state mass of $M_x > 15.7\,\text{GeV}$ were presented. Each measurement was extrapolated to the full LHC mass range and

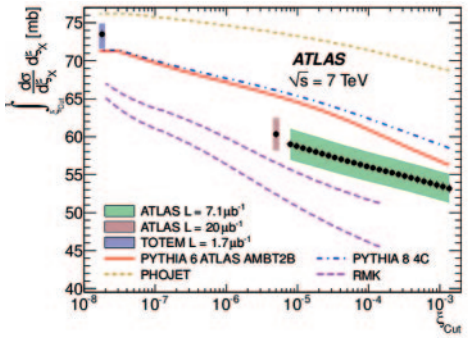

Fig. 8. – Differential inelastic cross section integrated on ξ over the mass range of the detector acceptance as a function of ξ. Data are compared to ATLAS results for the total inelastic cross section in the same mass range and to TOTEM measurement for low mass range.

compared to different MC generators. ATLAS measurement of the differential cross section as a function of the rapidity gap was also shown and used to validate the MC models used for the extrapolation to the full mass range. Even if the general trend of data was well described by the MCs, no model was currently able to reproduce the data in the whole η and ξ range for $\sqrt{s} = 7\,\text{TeV}$.

REFERENCES

[1] CMS Collaboration, *JINST*, **3** (2008) S08004.
[2] ATLAS Collaboration, *JINST*, **3** (2008) S08003.
[3] CMS Collaboration, *Phys. Lett. B*, **722** (2013) 5.
[4] CMS Collaboration, CMS-PAS-QCD-11-002 cdsweb.cern.ch/record/1433413.
[5] CMS Collaboration, CMS-PAS-FWD-11-001 cdsweb.cern.ch/record/1373466.
[6] ATLAS Collaboration, *Nat. Comm.*, **2** (2011) 463.
[7] Donnachie A. and Landshoff P. V., *Nucl. Phys. B*, **244** (1984) 322.
[8] Abbot B. *et al.* [D0 Coll], *Phys. Lett. B*, **440** (1998) 189; Abe F. *et al.* [CDF Coll], *Phys. Rev. Lett.*, **81** (1998) 5278, Adloff C. *et al.* [H1 Coll], *Eur. Phys. J. C*, **24** (2002) 517; Derrik M. *et al.* [ZEUS Coll], *Phys. Lett. B*, **369** (1996) 55.
[9] Achilli M. *et al.*, *Phys Rev D.*, **84** (2011) 094009.
[10] Block M. M. and Halzen F., *Phys. Rev. D*, **72** (2005) 036006.
[11] Shuler G. A. and Sjostrand T., *Phys. Rev. D*, **49** (1994) 2257.
[12] ATLAS Collaboration, *Eur. Phys. J. C*, **72** (2012) 1926.
[13] TOTEM Collaboration, *EPL*, **96** (2011) 21002.